IJST, Transactions of Civil and Environmental Engineering, Vol. 35, No. C1, pp 15-34
Printed in The Islamic Republic of Iran, 2011

A SANISAND-STRUCTURE INTERFACE MODEL*

A. LASHKARI

Dept. of Civil and Environmental Engineering, Shiraz University of Technology, I. R. of Iran
Email: lashkari_ali@hamyar.net

Abstract– The bearing capacity and deformation behavior of geostructures are highly dependent on the mechanical response of a thin layer of soil in contact with a structure that is technically called an interface. This paper presents a constitutive model for the mechanical behavior of sand-structure interfaces. To this goal, the critical state compatible bounding surface framework of Manzari & Dafalias is modified to capture the fundamental state dependent aspects of sand-structure interface behavior. The model has relatively few parameters which have clear physical meanings. The model predictions are compared with experimental results for various interface types, normal stress levels, and stiffness boundary conditions. Using a unique set of model parameters, it is shown that the model is capable of providing reasonable predictions for stress-displacements and normal displacement-tangential displacement behaviors of sand-structure interfaces.

Keywords– Interface, sand, state parameter, critical state, constitutive model, bounding surface, SANISAND

1. INTRODUCTION

In the design of most of earth structures like piles, shallow foundations, retaining walls, underground structures, and reinforced soils, an understanding of the mechanism of interaction between soil and structure is essential. In other words, to have a safe design, knowledge on the load-displacement behavior and the ultimate capacity to transfer loads from one medium to the other one is necessary. In the above geostructures, a very thin layer of soil adjacent to the structure surface, the so-called soil-structure interface, plays the most important role. Generally, the mechanical response of a soil-structure interface is significantly influenced by soil properties such as density, grain size distribution, mineralogy, and crushability as well as the type of loading, the boundary condition of the structure stiffness, and finally, the relative surface roughness [1-7].

Constitutive modeling of interface behavior is a relatively a new matter. In the literature, on the basis of various assumptions, a number of interface models have been suggested. Clough and Duncan [8] introduced an interface model based on the non-linear elasticity theory. Brandt [9] proposed a rigid-plastic constitutive model for soil-concrete interface. Within the elastoplasticity framework, Ghaboussi et al. [10] suggested an interface model using a cap yield surface. Among the recent works of this type, Ghionna and Mortara [6] proposed an elastoplastic interface model using a non-associated flow rule together with two Cam Clay type constitutive surfaces. Employing the disturbed state concept, several soil-structure interface models have been introduced [7, 11, and 12]. In the frameworks of generalized plasticity and critical state soil mechanics, recently, Liu et al. [13] and Liu and Ling [14] introduced interface models which are capable of predicting the behavior under various stress levels and densities. The latter model

*Received by the editors March 9, 2009; Accepted April 13, 2010.

considers the effect of particle breakage on the interface behavior. More recently, Mortara et al. [15] suggested an advanced interface model in the bounding surface plasticity context.

Manzari and Dafalias [16] introduced a stress ratio based bounding surface plasticity model, the so-called SANISAND (Simple ANIsotropic SAND) model, for the state dependent aspects of sand behavior such as dilatancy and peak shear stress. Using the Been and Jefferies [17] state parameter, the critical state compatible model of Manzari and Dafalias [16] is capable of distinguishinig dense samples from loose ones and providing realistic predictions for stress-strain-strength behavior of sands. Since its first proposal, this family of sand models has been widely developed and applied to various subjects. Among them, Papadimitriou and Boukovalas [18] and Dafalias and Manzari [19] considered the effect of stress induced anisotropy and significantly improved the capability of the basic model under cyclic loading. Li and Dafalias [20], Dafalias et al. [21], and Loukidis and Salgado [22] considered the effect of inherent anisotropy on sand stress-strain-strength behavior. Lashkari and Latifi [23] suggested a modified SANISAND model for non-coaxial flow of sand subjected to rotation of principal stress axes. Sadrnejad [24] introduced a SANISAND multi-plane model. Lashkari [25] proposed a modified SANISAND model for sand liquefaction under rotational shear. Taiebat and Dafalias [26] modified the basic SANISAND model in order to account for particle crushing under high confining pressures. Finally, Chiu and Ng [27] proposed a SANISAND model for unsaturated sands.

This study introduces a modified SANISAND model for soil-structure interfaces, the so-called SANISAND-structure interface model, which is built upon the recent work of Manzari and Dafalias [19]. The model calibration method is described in detail and the model simulative capacity is presented versus the experimental results of 26 tests reported by four independent research groups.

2. GENERAL FORMULATION OF THE MODEL

σ_n and τ are introduced, respectively, as normal and tangential stresses acting on the interface element (Fig. 1). For the mentioned configuration, the state of stress is illustrated by the following vector:

$$\{\boldsymbol{\sigma}\} = \begin{Bmatrix} \sigma_n \\ \tau \end{Bmatrix} \tag{1}$$

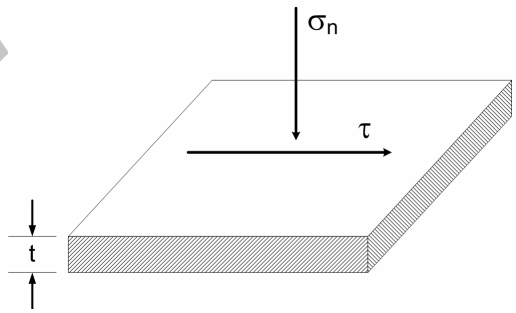

Fig. 1. Idealized representation of stresses acting on an interface

Strain rate vector corresponding to the rate of stress vector is defined by:

$$\{\dot{\boldsymbol{\varepsilon}}\} = \{\dot{\boldsymbol{\varepsilon}}\}^e + \{\dot{\boldsymbol{\varepsilon}}\}^p = \begin{Bmatrix} \dot{\varepsilon}_n \\ \dot{\varepsilon}_t \end{Bmatrix} = \begin{Bmatrix} \dot{\varepsilon}_n \\ \dot{\varepsilon}_t \end{Bmatrix}^e + \begin{Bmatrix} \dot{\varepsilon}_n \\ \dot{\varepsilon}_t \end{Bmatrix}^p \tag{2}$$

In above equation, strain rate vector is decomposed into elastic and plastic parts, respectively indicated by superscripts “e” and “p”.

The following constitutive law is taken from De Gennaro and Frank [28] to relate the rates of stress and elastic strain vectors:

$$\{\dot{\boldsymbol{\sigma}}\} = [\mathbf{D}]^{e} \{\dot{\boldsymbol{\varepsilon}}\}^{e} = \begin{bmatrix} K_n & 0 \\ 0 & K_t \end{bmatrix} \begin{Bmatrix} \varepsilon_n \\ \varepsilon_t \end{Bmatrix}^{e} \tag{3}$$

where K_n and K_t are normal and tangential stiffness moduli which must be stress dependent. In analogues to Hardin and Black [29] and Biarez and Hicher [30], it is suggested that:

$$K_n = K_{n0} \sqrt{\frac{\sigma_n}{p_{atm}}} \quad ; \quad K_t = K_{t0} \sqrt{\frac{\sigma_n}{p_{atm}}} \tag{4}$$

where K_{n0} and K_{t0} are material parameters and p_{atm} is a reference pressure which herein is taken as the atmospheric pressure (i.e., 101 kPa).

In the elastoplasticity theory, the plastic branch of strain rate vector is calculated by:

$$\{\dot{\boldsymbol{\varepsilon}}\}^{p} = \begin{Bmatrix} \dot{\varepsilon}_n^{p} \\ \dot{\varepsilon}_\tau^{p} \end{Bmatrix} = \Lambda \{\mathbf{R}\} = \Lambda \begin{Bmatrix} R_n \\ R_t \end{Bmatrix} \tag{5}$$

In above equation, $\{\mathbf{R}\}$ is a vector which defines the plastic strain rate direction and Λ, the so-called loading index, is a scalar-valued parameter which gives the instantaneous magnitude of plastic strain rate vector. The loading index is obtained from:

$$\Lambda = \frac{\{\mathbf{n}\}^{T} \{\dot{\boldsymbol{\sigma}}\}}{K_p} \tag{6}$$

where $\{\mathbf{n}\} = \partial f / \partial \boldsymbol{\sigma}$ is the normal vector to the yield surface which defines the direction of loading in stress space, and K_p is plastic hardening modulus. Special definitions of the model of this study for these terms are presented in sections 3 and 4. Considering Eqs. (3), (5) and (6), the following equation is obtained for Λ:

$$\Lambda = \frac{\{\mathbf{n}\}^{T} [\mathbf{D}]^{e} \{\dot{\boldsymbol{\varepsilon}}\}}{K_p + \{\mathbf{n}\}^{T} [\mathbf{D}]^{e} \{\mathbf{R}\}} \tag{7}$$

At this stage, by considering Eqs. (2), (3), and (7) together with some ordinary mathematical operations and rearrangement of terms, the elastoplastic stiffness matrix becomes:

$$\{\dot{\boldsymbol{\sigma}}\} = [\mathbf{D}]^{ep} \{\dot{\boldsymbol{\varepsilon}}\} \quad ; \quad [\mathbf{D}]^{ep} = [\mathbf{D}]^{e} - \frac{[\mathbf{D}]^{e} \{\mathbf{R}\} \{\mathbf{n}\}^{T} [\mathbf{D}]^{e}}{K_p + \{\mathbf{n}\}^{T} [\mathbf{D}]^{e} \{\mathbf{R}\}} \tag{8}$$

Various experimental studies indicated that the interface thickness is about 5 to 9 times of the mean grain diameter of soil in contact with the structure. Herein, the following empirical correlation is adopted for interface thickness [1, 3, and 7]:

$$t \approx 5\, d_{50} \tag{9}$$

where d_{50} is the mean grain diameter of sand. Now, by using Eq. (9), deformation components within the interface zone are calculated by [7, 13]:

$$\begin{Bmatrix} v \\ u \end{Bmatrix} = t \begin{Bmatrix} \varepsilon_n \\ \varepsilon_t \end{Bmatrix} \tag{10}$$

In Eq. (10), v and u are respectively the normal and tangential displacements.

3. SPECIAL FORMULATION OF THE MODEL

Yield surface designates the boundary of pure elasticity. In the τ-σ_n plane, the yield surface is a narrow wedge-shaped region (Fig. 2). Herein, the yield surface is defined by the following mathematical expression:

$$f = |\eta - \alpha| - m = 0 \tag{11}$$

In Eq. (11), $\eta\,(=\tau/\sigma_n)$ is the stress ratio, and α, the so-called back-stress ratio, is the angle which the bisector of the yield surface makes the positive direction of the σ_n axis (Fig. 2). For an isotropic interface which previously was not subjected to tangential stress, $\alpha = 0$. When an interface is subjected to monotonic tangential stress, α gradually increases due to the kinematic (rotational) hardening of the yield surface. Finally, m, a model parameter, indicates the yield surface size. Unlike cohesive soils, in granular media, the size of the yield surface is quite small. For practical purposes, $m = 0.01\,M$ is a reasonable assumption [19], where M is the slope of the critical state line measured in τ-σ_n plane (Fig. 2).

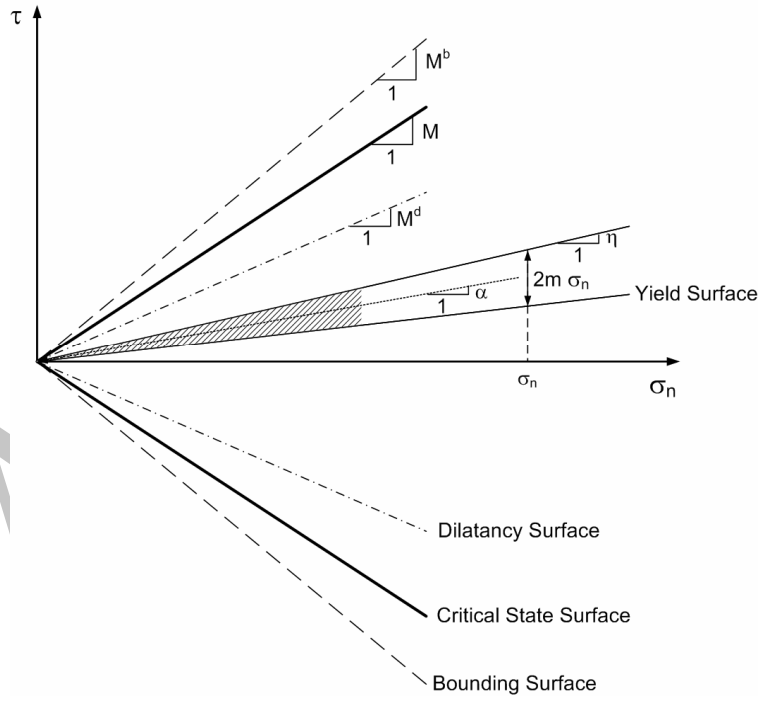

Fig. 2. Schematic view of the yield, bounding, critical, and dilatancy surfaces in τ-σ_n plane (after Dafalias and Manzari [19])

When the stress state reaches the yield surface, the mechanical response becomes a combination of elastic and plastic displacements. Under this condition, the normal vector to the yield surface is in the following form:

$$\{\mathbf{n}\} = \begin{Bmatrix} n_n \\ n_\tau \end{Bmatrix} \tag{12}$$

where its components are:

$$n_n = \frac{\partial f}{\partial \sigma_n} = -(s\alpha + m)$$
$$n_\tau = \frac{\partial f}{\partial \tau} = s \tag{13}$$

In above equations, $s = +1$ when $\tau = \alpha + m$ (i.e., shear takes place towards the compression side), whereas $s = -1$ when $\tau = \alpha - m$ (i.e., shear takes place towards the extension side).

In general, the assumption of normality is not valid for granular materials. This means that $\{\mathbf{R}\} \neq \{\mathbf{n}\}$, and as a result, the model flow rule must be of non-associated type. Herein, the non-associated flow rule of Dafalias and Manzari [19] is adopted:

$$\{\mathbf{R}\} = \begin{Bmatrix} d \\ n_\tau \end{Bmatrix} \tag{14}$$

In Eq. (14), the term d is the dilatancy function that is defined in section 4.

Using Eqs. (13) and (14) together with Eqs. (7) and (8), the loading index and elastoplastic stiffness matrix become:

$$\Lambda = \frac{sK_t\dot{\varepsilon}_\tau - (s\alpha + m)K_n\dot{\varepsilon}_n}{K_p + K_t - (s\alpha + m)K_n d}$$
$$[\mathbf{D}]^{ep} = \begin{pmatrix} K_n & 0 \\ 0 & K_t \end{pmatrix} - \frac{1}{K_p + K_t - (s\alpha + m)K_n d} \begin{pmatrix} -d(s\alpha + m)K_n^2 & sdK_nK_t \\ -(\alpha + sm)K_nK_t & K_t^2 \end{pmatrix} \tag{15}$$

In a special case, for monotonic loading in the compression side (i.e., $\tau \geq 0$), Eq. (15) can be further simplified:

$$\Lambda = \frac{K_t\dot{\varepsilon}_\tau - \eta K_n\dot{\varepsilon}_n}{K_p + K_t - \eta K_n d}$$
$$[\mathbf{D}]^{ep} = \begin{pmatrix} K_n & 0 \\ 0 & K_t \end{pmatrix} - \frac{1}{K_p + K_t - \eta K_n d} \begin{pmatrix} -d\eta K_n^2 & dK_nK_t \\ -\eta K_nK_t & K_t^2 \end{pmatrix} \tag{16}$$

Yield surface always holds the stress state in such a way that the stress point may not slip beyond its domain. In practice, this goal is achieved by imposing the consistency condition:

$$df = \frac{\partial f}{\partial \sigma_n}\dot{\sigma}_n + \frac{\partial f}{\partial \tau}\dot{\tau} + \frac{\partial f}{\partial \alpha}\dot{\alpha} = 0 \tag{17}$$

Considering Eqs. (11) and (13), one has

$$df = n_n\dot{\sigma}_n + n_\tau\dot{\tau} - s\sigma_n\dot{\alpha} = 0 \tag{18}$$

Hence, with respect to Eq. (6), the rate of α is:

$$\dot{\alpha} = \frac{n_n\dot{\sigma}_n + n_\tau\dot{\tau}}{s\sigma_n} = \frac{\Lambda K_p}{\sigma_n}s \tag{19}$$

Similar to the other members of the SANISAND family, in addition to the yield surface, the model has three other constitutive surfaces: bounding surface, critical state surface, and dilatancy surface (Fig. 2). As implied by its name, the bounding surface defines a boundary on the evolution of stress due to kinematic hardening and as a result, corresponds to a domain for all permissible stress states. Critical state surface (defined by $\tau = M\,\sigma_n$ in τ-σ_n plane) is the terminal loci of all samples reaching critical state. Finally, the dilatancy surface is a reference state boundary which dictates the type and magnitude of the plastic volume change. An interface is in loose state and contracts due to shearing when the current stress state is inside the dilatancy surface. On the other hand, the mentioned interface dilates when its corresponding stress state is located beyond the dilatancy surface. The critical state surface size remains unchanged during shearing; however, the sizes of bounding and dilatancy surfaces are direct functions of the interface state. This issue is further discussed in the following section.

4. STATE DEPENDENT SAND-STRUCTURE INTERFACE BEHAVIOR

Regarding volume change, hardening, and residual strength, experimental investigations revealed the similarities between the mechnical responses of the sand-structure interfaces and pure granular media [3, 7]. As a consequence, some researchers suggest that the concept of critical state soil mechanics can be extended to the soil-structure interfaces [7, 13]. From this viewpoint, for an interface, the critical state can be defined as a state at which the interface continues tangential displacement at constant amounts of normal stress, tangential stress, and normal deformation.

In this model, dilatancy, d, and plastic hardening modulus, K_p, are direct functions of the interface state:

$$d = A(\alpha^d - s\alpha) \tag{20}$$

$$K_p = h_0 K_t \frac{(\alpha^b - s\alpha)}{|\alpha - \alpha_{in}|} \tag{21}$$

where A and h_0 are model parameters. α_{in} is the instantaneous amount of α when the most recent tangential loading starts. α^b and α^d are back-stress ratios associated with bounding and dilatancy surfaces, respectively:

$$\begin{aligned} \alpha^b &= M^b - m \\ \alpha^d &= M^d - m \end{aligned} \tag{22}$$

In Eq. (22), M^b and M^d indicate respectively the sizes of bounding and dilatancy surfaces (Fig. 2). According to Dafalias and Manzari [19], M^b and M^d are related to the interface state through:

$$\begin{aligned} M^b &= M\exp(-n^b\,\psi) \\ M^d &= M\exp(n^d\,\psi) \end{aligned} \tag{23}$$

where n^b and n^d are model parameters, and $\psi = e - e_c$ is the modified state parameter of Been and Jefferies [17]. In the definition of a state parameter, e and e_c are the current and critical state void ratios. The location of the critical state line in the e-σ_n plane is defined by:

$$e_c = e_0 - \lambda \ln(\sigma_n / p_{atm}) \tag{24}$$

where e_0 and λ are model parameters. e_0 is the value of the critical void ratio at reference atmospheric pressure. Definition of the modified ψ is demonstrated in Fig. 3.

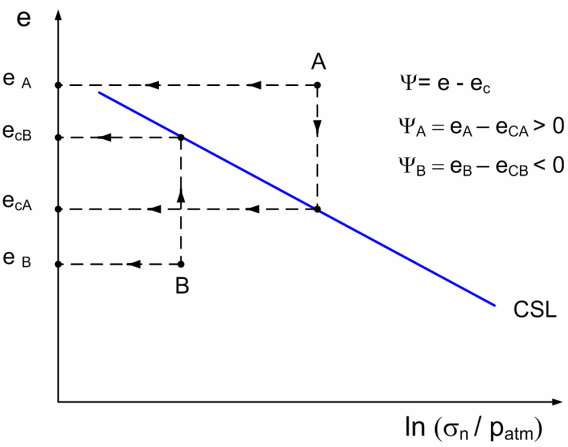

Fig. 3. Definition of state parameter for sand-structure interfaces

5. THE MODEL CALIBRATION

A total of nine parameters are required to be determined for complete calibration of the SANISAND-structure interface model. Divided into five categories, as listed in the following, all model parameters have clear physical meanings and a systematic straightforward calibration method exists for each. To determine the model parameters, the following procedures are recommended:

a) Elastic parameters

K_{t0} and K_{n0} are related to the elastic portion of behavior. K_{t0} can be calibrated by constructing a tangent line to the very beginning parts of shear stress versus tangential displacement curves in constant normal stress tests. In the same manner, K_{n0} can be determined by tangent to the very beginning parts of normal stress versus normal deformation curves in pure compression tests. Thus, with respect to Eqs. (3), (4), and (10), K_{t0} and K_{n0} can be calculated by:

$$K_{t0} = t\sqrt{\frac{p_{atm}}{\sigma_n}}\left(\frac{\delta\tau}{\delta u}\right)$$
$$K_{n0} = t\sqrt{\frac{p_{atm}}{\sigma_n}}\left(\frac{\delta\sigma_n}{\delta v}\right) \qquad (25)$$

Hereafter, δ indicates the increment of the related parameter.

b) Critical state line parameters

M, e_0 and λ were introduced to define the location of the critical state line. For a number of tests reaching critical state, M is the slope of the best fitted line crossing the origin in the τ-σ_n plane. In the e-σ_n plane, one can use the same ordinary statistical procedure to determine e_0 and λ. To this aim, critical void ratios must be plotted against $ln(\sigma_n / p_{atm})$. Once the best fitted line is drawn, e_0 and λ are the intercept with the e-axis and the slope of the best fitted line, respectively.

c) Parameters of state dependency

The sizes of bounding and dilatancy surfaces are direct functions of the interface state. Similar to Dafalias and Manzari [19], n^b and n^d are categorized as the parameters of the sand-structure interface state. Following the same path as that followed in the last sub-section leads to the calculation of n^b and n^d. Considering Eqs. (23), one has:

$$n^d = \frac{1}{\psi}\ln\left(\frac{M^d}{M}\right)$$
$$n^b = \frac{-1}{\psi}\ln\left(\frac{M^b}{M}\right) \quad (26)$$

Hence, n^d is the slope of the best fitted line plotted using data of $ln(M^d/M)$ versus ψ. The same method using the data of $-ln(M^b/M)$ against ψ leads to n^b.

d) Dilatancy parameter

In the model presented, *A* controls the instantaneous magnitude of dilatancy. Ignoring the small contribution of elastic strains in moderate deformations, one can assume:

$$d = \frac{\dot{\varepsilon}_v^p}{\dot{\varepsilon}_\tau^p} \approx \frac{\delta\varepsilon_v}{\delta\varepsilon_\tau} = \frac{\delta v}{\delta u} \quad (27)$$

Hence, with respect to Eq. (20), one has:

$$A \approx \frac{1}{(M^d - \eta)} \cdot \frac{\delta v}{\delta u} \quad (28)$$

By using data from the constant normal stress or constant stiffness tests together with Eq. (28), one can calculate *A* for some tests and use the average value.

e) Hardening parameter

Using the data of the constant normal stress tests, one can estimate the value of h_0 by the following procedure. For a normal stress test in the compression side, it can be shown that:

$$\dot{\varepsilon}_\tau = \left(\frac{1}{K_t} + \frac{1}{K_p}\right)\dot{\tau} \quad (29)$$

At this point, using a definition of the plastic modulus given in Eq. (21), one has:

$$h_0 = \frac{1}{(\frac{M_b}{\eta} - 1)(K_t \frac{\delta\varepsilon_\tau}{\delta\tau} - 1)} \quad (30)$$

6. THE MODEL VALIDATION

This section is organized to present the simulative capability of the SANISAND-structure interface model. To this aim, the model predictions are compared with the results of experiments reported by four independent research groups for various interface types, stress levels, and stiffness boundary conditions.

It has been shown that the stiffness boundary condition imposed by the structure in contact with soil mass has a great influence on the interface response [3, 6, and 28]. The stiffness in the direction normal to the interface is usually denoted by K through the following constitutive relationship:

$$\dot{\sigma}_n = -K\,\dot{v} \quad (31)$$

where $\dot{\sigma}_n$ and $\dot{v}$ are the rates of the normal components of the stress and displacement vectors, respectively. As stated by Evgin and Fakharian [3], three typical boundary conditions are generally assigned in experimental studies:

- K= 0, i.e., $\dot{\sigma}_n = 0\,;\ \dot{v} \neq 0$ (constant normal stress condition)
- K= ∞, i.e., $\dot{\sigma}_n \neq 0\,;\ \dot{v} = 0$ (constant volume condition)
- K= constant, i.e., $\dot{\sigma}_n \neq 0\,;\ \dot{v} \neq 0$ (constant normal stiffness condition)

a) First set of comparisons

Evgin and Fakharian [3] published an extensive set of experiments on Ottawa sand, a coarse silica sand, in contact with low carbon rough steel plate in a modified simple shear interface apparatus, the so-called C3DSSI. All samples were deposited using multiple-sieving-pluviation method with the relative density D_r= 84 % (namely e ≈ 0.696). The physical properties of Ottawa sand are given in Table 1. Steel plates have a surface roughness R_{max} of 25 μm in a sampling length of 0.8 mm.

Table1. Physical properties of Ottawa§, Yongdinghe¶ , Toyoura¥ , and Hostun★ sands
(§:Evgin and Fakharian [3]; ¶:Hu and Pu [7]; ¥:Fioravante [31]; ★:Shahrour and Rezaie[5])

Granular material	Mean diameter, d_{50} (mm)	Uniformity coefficient, U_c	Maximum void ratio, e_{max}	Minimum void ratio, e_{min}	Specific gravity, G_s	Mineralogy	Angularity
Ottawa sand	0.6	-	1.024	0.651	2.65	quartz	angular
Yongdinghe sand	1.0	2.1	1.026	0.654	2.65	quartz	angular
Toyoura sand	0.22	1.3	1.024	0.643	2.65	quartz (90%) feldspar 10%)	subangular
Hostun sand	0.32	1.7	1.00	0.653	2.65	quartz	angular

Using the calibration method described in the last section, the model is calibrated versus the 2D interface tests reported by Evgin and Fakharian [3]. Fig. 4 illustrates the calibration process for K_{t0}, M, e_0, λ, n^b, and n^d. Amounts of model parameters in this set of simulations are presented in Table 2.

Table 2. Amounts of model parameters used in simulations

Interface type	Elasticity *		Critical state line			State		Dilatancy	Hardening
	K_{t0} (MPa)	K_{n0} (MPa)	M	e_0	λ	n^b	n^d	A	h_0
Ottawa sand-steel	5.0	5.85	0.638	1.010	0.090	1.15	0.73	0.75	0.35
Yongdinghe sand-steel	4.4	5.15	0.610	1.033	0.033	2.10	0.50	0.63	0.20
Toyoura sand-aluminum	1.5	1.75	0.670	1.011	0.107	2.20	2.00	0.55	0.20
Hostun sand-steel	3.0	3.6	0.640	0.850	0.047	1.80	1.00	0.60	0.60

*: p_{atm} = 101 kPa

For three constant normal stress tests (K=0) with σ_n= 100, 300, and 500 kPa, the model simulations are compared with experiments in Fig. 5. For three constant stiffness tests (K= 800 MPa/m) with different amounts of initial normal stress (σ_n= 100, 200, and 300 kPa), the model predictions are illustrated versus experiments in Fig. 6. To explore the simulative capability of the model on the effect of varying stiffness, predictions for K=0, 200, 400, 600, 800, and 1200 MPa/m are shown against the experimental results in Fig. 7. For K= 400, 800, and 1200 MPa/m cases, a comparison of the predicted and measured stress paths are shown in Fig. 8.

As it is observed, overall, the model is capable of accounting for the general state dependent behavior of sand-steel interface tests reported by Evgin and Fakharian [3].

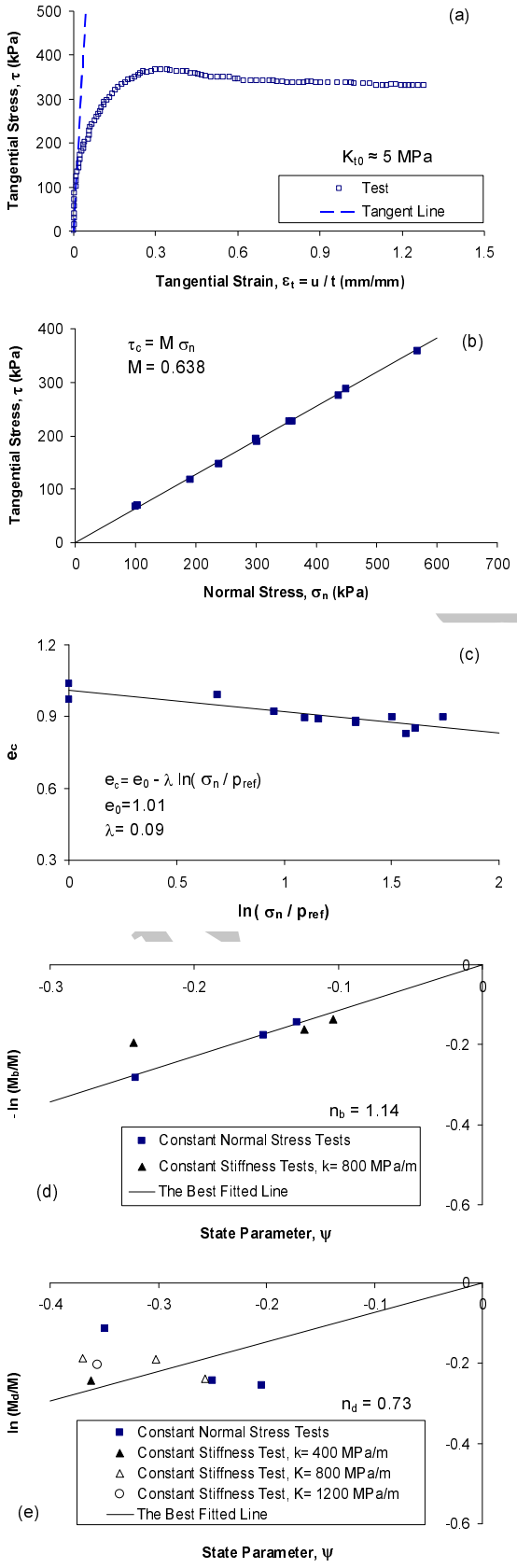

Fig. 4. Calibration of K_{t0}, M, e_0, λ, n_b, and n_d for Ottawa sand-steel interface (experimental data reported by Evgin and Fakharian [3])

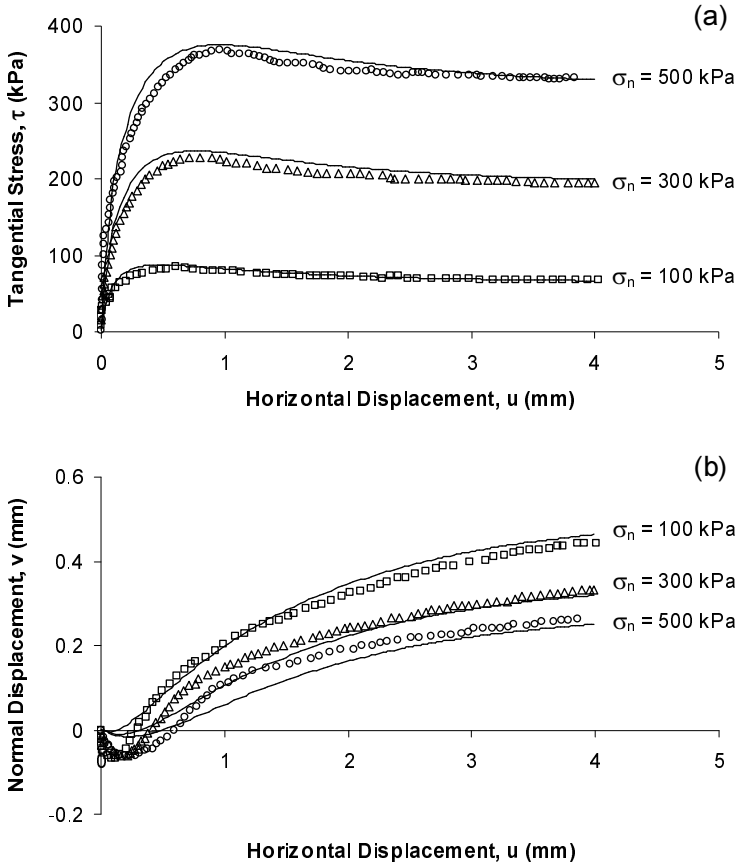

Fig. 5. Comparison of model predictions with experiments for three constant normal stress Ottawa sand-steel interface tests reported by Evgin and Fakharian [3]

b) Second set of comparisons

Hu and Pu [7] carried out a series of interface tests using direct shear apparatus to investigate the mechanical behavior of Yongdinghe sand-steel interface. Samples were air-pluviated with the relative density D_r= 90 % (namely e ≈ 0.691). The physical properties of Yongdinghe sand are given in Table 1. In tests, rough (R_{max}= 0.5 mm in sampling length of 1 mm) low-carbon steel plates were grooved in the direction normal to shearing direction.

For four constant normal stress tests, the comparison of the model predictions with the test results is demonstrated in Fig. 9. The testing program covers a wide range of normal stresses. As presented, the SANISAND-structure model renders satisfactory simulations. In the simulations presented, the amounts of model parameters are given in Table 2.

c) Third set of comparisons

Ghionna and Mortara [6] reported the results of their experiments on the mechanical behavior of Toyoura sand-aluminum (so-called ToD60) interface using direct shear apparatus. The physical properties of Toyoura sand are given in Table 1. Toyoura sand samples were prepared in dense state with D_r= 85 % (e ≈ 0.70), and aluminum plates were categorized rough (R_{max}= 60 μm).

Using two samples subjected to tangential shear with K= 0 and 1000 MPa/m, the model was calibrated and then was used for simulation of the other tests. In the simulations presented, the amounts of the model parameters are given in Table 2 and the thickness of the interface was taken 2.3 mm. Fig. 10 illustrates comparisons between the model predictions against experiments for tests used in calibration. For three constant normal stress tests with σ_n= 100, 200, and 300 kPa, the model predictions are shown

together with the experiments in Fig. 11(a). In addition, for three constant normal stiffness tests (K= 1000 MPa/m), the predicted stress paths are demonstrated versus the measured results in Fig. 11(b).

Comparison of predictions with experiments indicates that the model can provide satisfactory results, even when limited data are available for the model calibration.

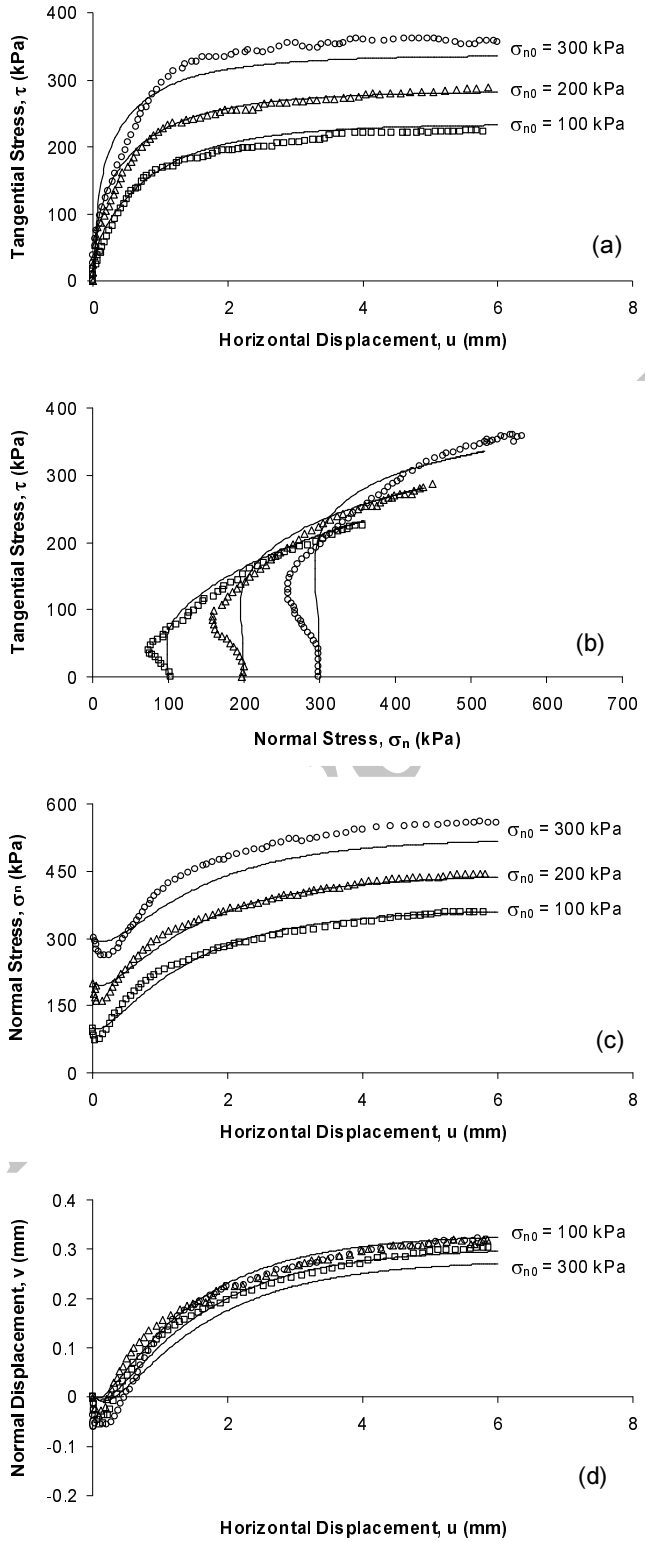

Fig. 6. Comparison of model predictions with experiments for three constant stiffness tests with K= 800 MPa/ m on Ottawa sand-steel interface reported by Evgin and Fakharian [3]

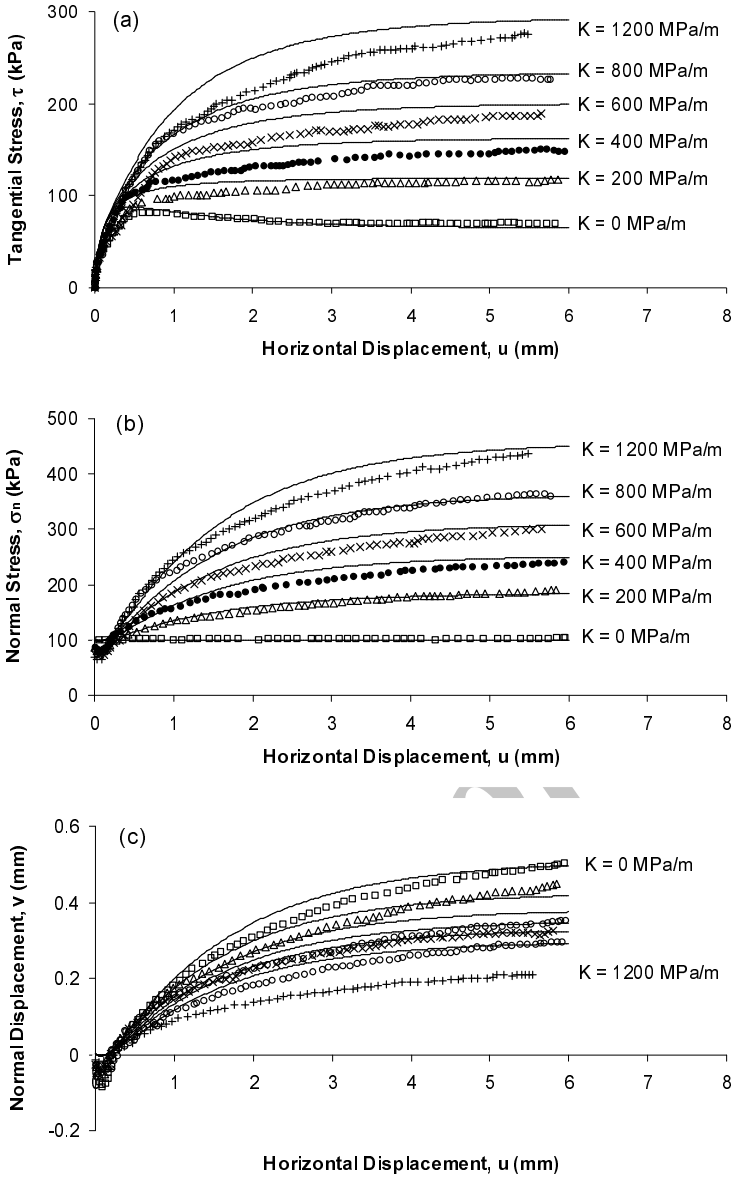

Fig. 7. Comparison of model predictions with experiments for six constant stiffness Ottawa sand-steel interface (K = 0 - 1200 MPa/m and σ_{n0}= 100 kPa) tests (experimental data reported by Evgin and Fakharian [3])

d) Fourth set of comparisons

Using a modified direct shear apparatus, Shahrour and Rezaie [5] studied the mechanical behavior of Hostun sand- rough steel interfaces prepared in dense (D_r=90%) and very loose (D_r=15%) states. The physical properties of Hostun sand are given in Table 1. Using this set of experiments, the model was calibrated. The amounts of model parameters are given in Table 2. It is worth mentioning that the interface thickness is assumed 7 mm in all predictions.

For six dense and very loose samples of Hostun sand-steel interfaces subjected to constant normal stress condition, the model predictions are compared with experimental data for σ_n=100, 200, and 300 kPa in Fig. 12. The model predicted a peak in the shear strength of each dense interface. On the other hand, the model correctly predicted that the peak does not take place for interfaces in loose state, and for such

samples, the maximum tangential strengths are attained at large tangential displacements. Moreover, considering the normal displacements-tangential displacement curves, the model predicted initial contraction, which turned into dilation in moderate tangential displacements for interfaces in dense state. A reverse manner is observed for interfaces in loose state, which demonstrate continuous contraction during shear. It is observed that the model predictions are in good agreement with the experimental data.

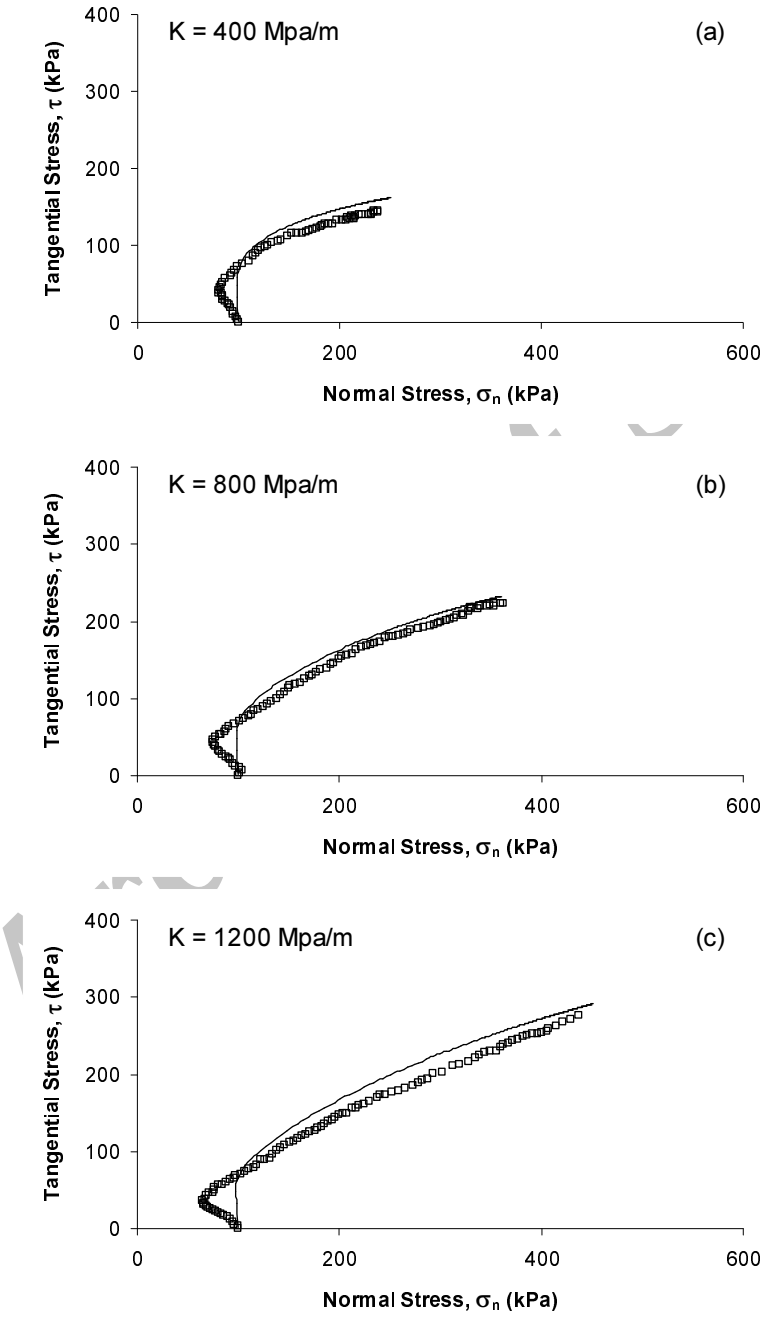

Fig. 8. Comparison of predicted stress paths with measured results for three constant stiffness Ottawa sand-steel interface (K = 400, 800, and 1200 MPa/m and σ_{n0}= 100 kPa) tests (experimental data reported by Evgin and Fakharian [3])

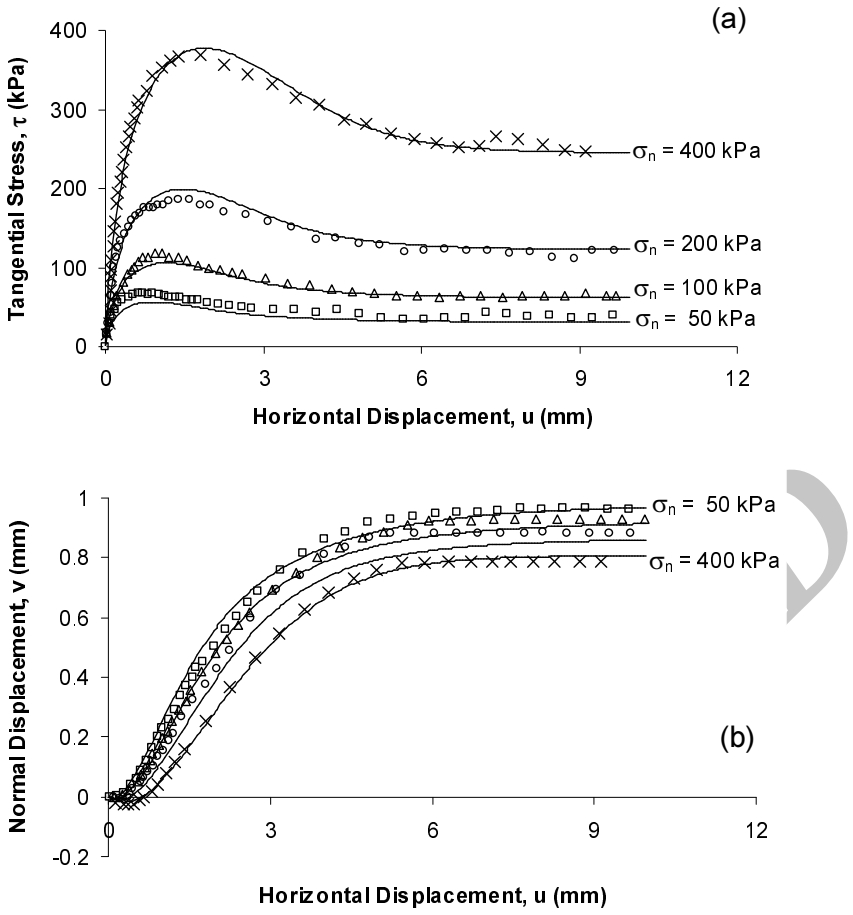

Fig. 9. Comparison of model predictions with experiments for four constant normal stress Yongdinghe sand-steel interface tests reported by Hu and Pu [7]

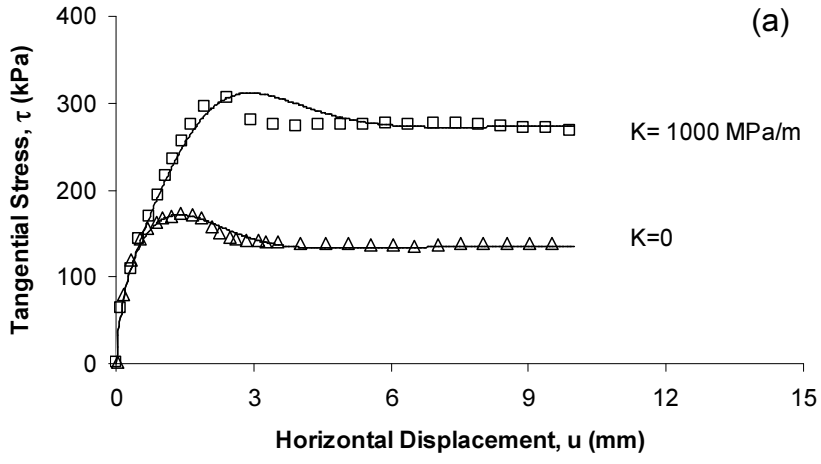

Fig. 10. Comparison of model predictions with experiments for two Toyoura sand-aluminum interface tests reported by Mortara et al. [14]

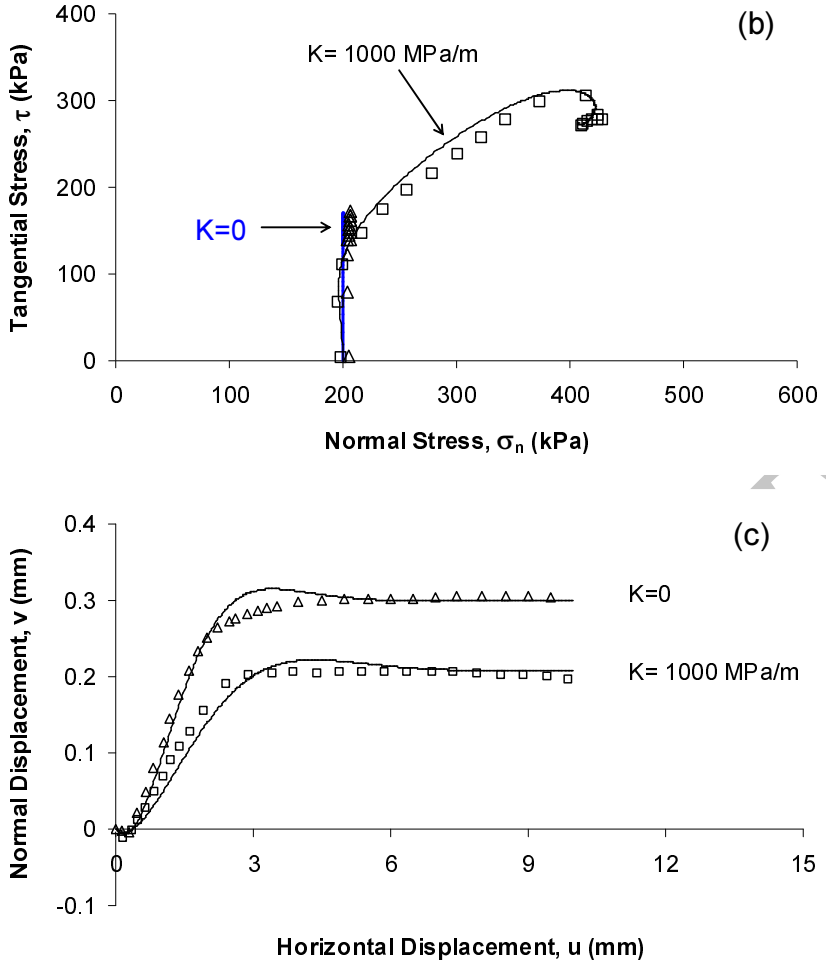

Fig. 10. Continued

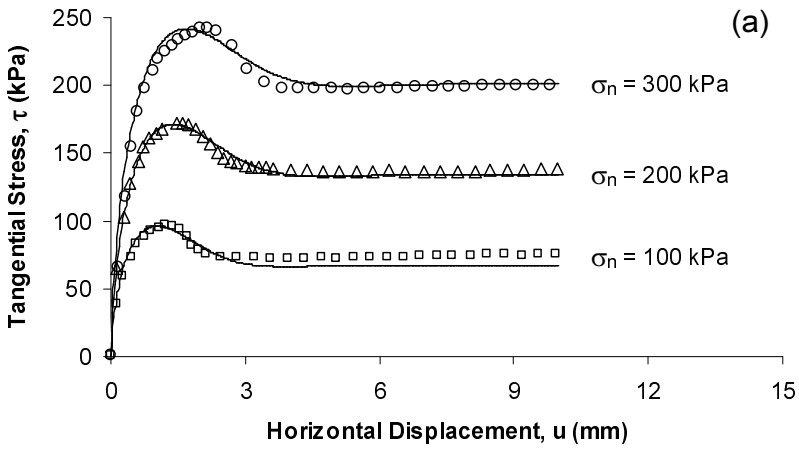

Fig. 11. Comparison of model predictions with experiments on Toyoura sand-aluminum interface for: (a) three constant normal stress tests (K=0), (b) three constant normal stiffness tests (K=1000 MPa/m) (data reported by Ghionna and Mortara [6])

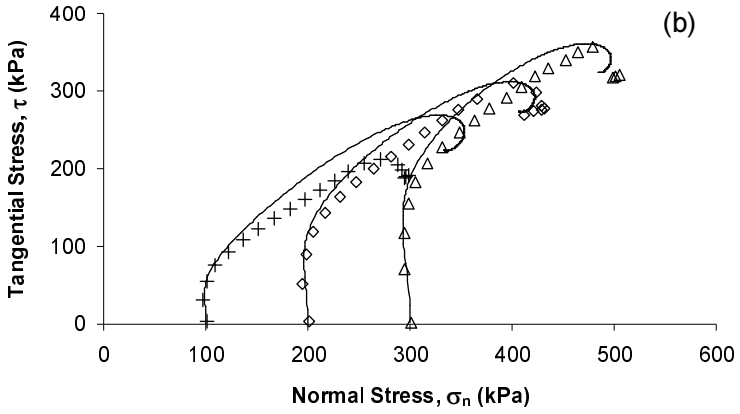

Fig. 11. Continued

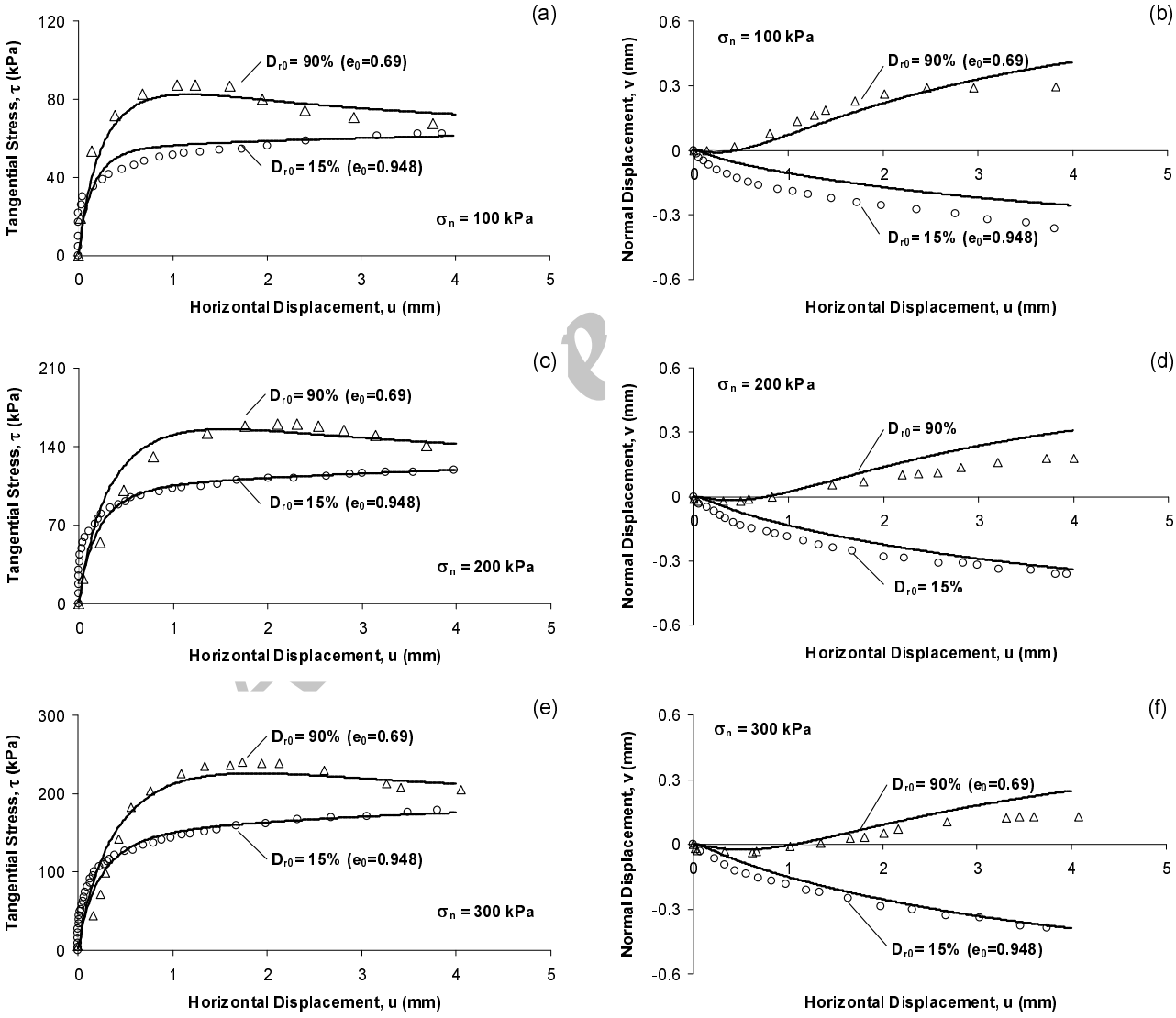

Fig. 12. Comparisons of the model predictions with experiments for initially dense (D_r= 90 %) and very loose (D_r=15 %) samples of Hostun sand-steel interfaces subjected to constant normal stress tests with different amounts of normal stresses: (a and b) σ_n=100 kPa, (c and d) σ_n=200 kPa, (e and f) σ_n=300 kPa (data reported by Shahrour and Rezaie [5])

7. CONCLUDING REMARKS

A constitutive model for simulation of sand-structure interfaces behavior was introduced within the SANISAND framework. As a mutual point between all SANISAND-based models, the presented model consists of a bounding surface, a narrow yield surface, dilatancy, and critical state surfaces. Among them, the yield surface may be subjected to kinematic hardening associated with shearing. Similar to the other members of the SANISAND family, the sizes of bounding and dilatancy surfaces are direct functions of the interface state. To this aim, the concept of state parameter [17] was used as an index of the current state. Due to the particular definitions of the bounding and dilatancy surfaces, both dilatancy and plastic hardening modulus are state dependent. The mentioned definitions significantly enhance the model capability to capture the state dependent aspects of interface behavior such as phase transformation and peak shear strength. The model formulation, calibration method, and the model evaluation were presented in detail. Having a simple formulation together with a reasonable number of parameters, it was shown that the model is capable of simulating general sand-structure interface behavior. The model predictions are compared with 26 tests reported by four independent research teams. As an important advantage, the model can predict the mechanical response of interfaces in wide ranges of states (wide ranges of densities, and applied normal stresses) using a unique set of parameters. Technically, direct incorporation of Been and Jefferies [17] state parameter in the model formulation has given the mentioned ability to the model to predict the state dependent behavior of interfaces without the need to change parameters. It must be mentioned that those models which do not include the state parameter in their formulations (such as [5-12]) may not be used for prediction of the mechanical behavior of interfaces over wide ranges of normal stresses and densities.

The model limitations are also discussed here for future improvement. Experimental findings have revealed that roughness may have influence on the interface friction angle. M increases in a linear manner with roughness when normalized roughness is less than a critical threshold which is called critical roughness. For amounts of roughness larger than the critical value, interface friction angle reaches a saturated state and remains constant [1, 7, 32, and 33]. Moreover, Hu and Pu [7] and Porcino et al. [33] reported that a similar mechanism governs the volume change behavior of interfaces. They observed that the stress-strain behavior of smooth interfaces follows an elastic-perfectly plastic pattern, and the generated normal displacement is very small. Hence, it is logical to assume that dilatancy and the location of the critical state line in e-σ_n plane are functions of the interface normalized roughness when roughness is less than critical normalized roughness. At this stage, it can be concluded that the model of this study can confidently be used for rough interfaces. For smooth and intermediate interfaces, the model of this study can be applied only when the variation of roughness is negligible (namely the influence of roughness is taken into account during calibration). When variation of roughness is considerable, one can improve the model capability by the use of an existing approach like that of Liu et al. [13].

Besides, studies using modified simple shear device (e.g., [3]) reported strong contraction immediately after the start of shearing. This contraction may not be predicted by the model in this study and almost all of the other interface models in the literature (e.g., [5, 7, 12, and 13]). To explain this observation, Ghionna and Mortara [6] concluded that two different mechanisms govern the normal displacement behavior of sand-structure interfaces. Initially, interfaces show significant contraction due to a slip down like mechanism. Subsequently, the second mechanism takes place and contraction turns gradually into dilation when strong strain localization occurs. Based on their explanation, Ghionna & Mortara [6] suggested a bi-line flow rule. Regarding this issue, further improvement of the SANISAND-structure interface model is required.

Acknowledgement- The author wishes to acknowledge Dr. E. Seyyedi of Ferdowsi University and Mrs. B. Lashkari for critical review of the manuscript.

REFERENCES

1. Kishida, H. & Uesugi, M. (1987). Tests of interfaces between sand and steel in simple shear apparatus. *Géotechnique*, Vol. 37, No. 1, pp. 45-52.
2. Boulon, M. (1989). Basic features of soil structure interface behavior. *Computers and Geotechnics*, Vol. 7, pp. 115-131.
3. Evgin, E. & Fakharian, K. (1996). Effect of stress path on the behavior of sand-steel interface. *Can. Geotech. J.*, Vol. 33, pp. 853-865.
4. Evgin, E. & Fakharian, K. (1998). Cyclic rotational simple-shear behavior of sand-steel interface. *Soils and Foundations*, Vol. 38, No. 2, pp. 191-199.
5. Shahrour, I. & Rezaie, F. (1997). An elastoplastic constitutive relation for the soil-structure interface under cyclic loading. *Computers and Geotechnics*, Vol. 21, pp. 21-39.
6. Ghionna, V. N. & Mortara, G. (2002). An elastoplastic model for sand-structure interface behavior. *Géotechnique*, Vol. 52, No. 1, pp. 41-50.
7. Hu, L. & Pu, J. (2004). Testing and modeling of soil-structure interface. *ASCE J. Geotech. Geoenviron. Eng.*, Vol. 130, No. 8, pp. 851-860.
8. Clough, G. W. & Duncan, J. M. (1971). Finite element analysis of retaining wall behavior. *J. Soil Mech. & Found. Div. ASCE*, Vol. 97, No. SM12, pp. 1657-1672.
9. Brandt, J. R. T. (1985). Behavior of soil-concrete interfaces. Ph.D. Thesis, University of Alberta, Canada.
10. Ghaboussi, J., Wilson, E. L. & Isenberg, J. (1973). Finite element for rock joints and interfaces. *J. Soil Mech. & Found. Div. ASCE*, Vol. 99, No. SM10, pp. 833-848.
11. Navayogarajah, N., Desai, C. S. & Kiousis, P. D. (1992). Hierarchical single-surface model for static and cyclic behavior of interfaces. ASCE J. Engng. Mech., Vol. 118, No. 5, pp. 990-1011.
12. Desai, C. S. (2005). *Unified yet simplified disturbed state constitutive models for sand and interface/joints*. ASCE Geotechnical Special Publication No. 128. Eds. J. A. Yammamuro and V. N. Kaliakin, pp. 159-183.
13. Liu, H., Song, E. & Ling, H. I. (2006). Constitutive modeling of soil-structure interface through the concept of critical state soil mechanics. *Mechanics Research Communications*, Vol. 33, pp. 515-531.
14. Liu, H. & Ling, H. I. (2008). Constitutive description of interface behavior including cyclic loading and particle breakage within the framework of critical state soil mechanics. *Int. J. Numer. Anal. Meth. Geomech.*, Vol. 32, No. 12, pp. 1495- 1514.
15. Mortara, G., Boulon, M. & Ghionna, V. N. (2002). A 2-D constitutive model for cyclic interface behavior. *Int. J. Numer. Anal. Meth. Geomech*., Vol. 26, pp. 1071- 1096.
16. Manzari, M. T. & Dafalias, Y. F. (1997). A critical state two surface plasticity model for sands. *Géotechnique*, Vol. 47, No. 2, pp. 255-272.
17. Been, K. & Jefferies, M. G. (1985). A state parameter for sands. *Géotechnique*, Vol. 35, No. 2, pp. 99-112.
18. Papadimitriou, A. G. & Boukovalas, G. D. (2002). Plasticity model for sand under small and large cyclic strains: a multiaxial formulation. *Soil Dynamics and Earthquake Engineering*, Vol. 22, pp. 191-204.
19. Dafalias, Y. F. & Manzari, M. T. (2004). Simple plasticity sand model accounting for fabric change effects. *ASCE J. Engng. Mech*., Vol. 130, No. 6, pp. 622-634.
20. Li, X. S. & Dafalias, Y. F. (2002). Constitutive modeling of inherently sand behavior. *ASCE J. Geotech. Geoenviron. Eng*., Vol. 128, No. 10, pp. 868-880.
21. Dafalias, Y. F., Papadimitriou, A. G. & Li, X. S. (2004). Sand plasticity model accounting for inherent fabric anisotropy. *ASCE J. Engng. Mech*., Vol. 130, No. 11, pp. 1319-1333.

22. Loukidis, D. & Salgado, R. (2009). Modeling sand response using two-surface plasticity. *Computers and Geotechnics*, Vol. 36, pp. 166-186.
23. Lashkari, A. & Latifi, M. (2008). A non-coaxial constitutive model for sand deformation under rotation of principal stress axes. *Int. J. Numer. Anal. Meth. Geomech*., Vol. 32, No. 9, pp. 1051- 1086.
24. Sadrnejad, S. A. (2007). A general multi-plane model for post-liquefaction of sand. *Iranian Journal of Science & Technology, Transaction B, Engineering*, Vol. 31, No. B2, pp. 123-141.
25. Lashkari, A. (2009). A constitutive model for sand liquefaction under rotational shear. *Iranian Journal of Science & Technology, Transaction B, Engineering*, Vol. 33, No. B1, pp. 31-48.
26. Taiebat, M. & Dafalias, Y. F. (2008). SANISAND: Simple anisotropic sand plasticity model. *Int. J. Numer. Anal. Meth. Geomech.* Vol. 32, No. 8, pp. 915-948.
27. Chiu, C. F. & Ng, C. W. W. (2003). A state dependent elastoplastic model for saturated and unsaturated soils. *Géotechnique*, Vol. 53, No. 9, pp. 809-829.
28. De Gennaro, V. & Frank, R. (2002). Elasto-plastic analysis of the interface behavior between granular media and structure. *Computers and Geotechnics*, Vol. 29, pp. 547-572.
29. Hardin, B. O. & Black, W. L. (1969). Closure to vibration modulus of normally consolidated clays. *J. Soil Mech. & Found. Div. ASCE*, Vol. 95, No. SM6, pp. 1531–1537.
30. Biarez, J. & Hicher, P. Y. (1994). *Elementary mechanics of soil behavior*. A. A. Balkema, Rotterdam.
31. Fioravante, V. (2002). On the shaft friction modeling on non-displacement piles in sand. *Soils and Foundations*, Vol. 42, No. 2, pp. 23-33.
32. Yoshimi, Y. & Kishida, H. (1981). Friction between sand and metal surfaces. *Proceedings of 10th International Conference on Soil Mechanics and Foundation Engineering*, Stockholm, Sweden, Vol. 1, pp. 831–834.
33. Porcino, D., Fioravante, D., Ghionna, V. N. & Pedroni, S. (2003). Interface behavior of sands from constant normal stiffness direct shear tests. *ASTM Geotechnical Testing Journal*, Vol. 26, No. 3, pp. 1-13.